Optimizing Acoustic Signal Quality for Linear Optoacoustic Communication

Md Shafiqul Islam, Mohamed Younis, and Fow-Sen Choa Department of Computer Science and Electrical Engineering University of Maryland Baltimore County Baltimore, Maryland, USA mdislam1, younis, choa@umbc.edu

Abstract—In underwater wireless networks, optoacoustic energy conversion using high energy laser pulse is the only known viable option for communication from an airborne unit to a node at large depth, e.g., a submarine or an unmanned underwater vehicle. However, controlling the generated acoustic signal through this process is very complex. Specifically, if the repetition rate of laser pulses is low, the corresponding acoustic signal is very broadband. The higher frequency components of this broadband signal attenuate more if the underwater node is very far from the surface. Hence, a relatively narrowband signal with lower components is desirable for long distance communication. The frequency component of the broadband acoustic signal depends on the incident angle of the laser light and observation angle of the receiver, i.e., the position of the underwater hydrophone. Both of these angles also change continuously for a wavy water surface, which makes it more complex to determine the frequency components of this kind of signal. In this paper, we show that by carefully choosing the relative position of the airborne unit and underwater node, we can generate a narrowband acoustic signal with lower frequency components for both flat and wavy water surfaces. We provide theoretical analysis and simulation results to capture the effect of these angles on the generated acoustic signals. We further provide guidelines for optimum angle setting for improving the quality of the optoacoustic communication link.

Keywords—Underwater networks; Optoacoustic energy conversion; Underwater acoustic communication.

I. INTRODUCTION

Recent advances in acoustic communication technology make underwater wireless networks quite attractive for many application domains, especially in marine science, search and rescue and naval combat. However, communication from an airborne unit to an underwater node is still very challenging due to the lack of any suitable physical signal which propagates smoothly in both air and water medium. For example, radio frequency works well in air, yet the signal strength diminishes drastically as soon as it penetrates the water surface. While acoustic signals are usually used underwater environments [1][2], again they lose most energy when crossing the air-water interface. Given the transmissivity of light from air to water is very high, visible light, e.g., LED, and laser have been pursued for cross medium communication [3][4]. However, neither LED nor laser light is good for long range communication due to the high light absorption and beam scattering, especially for a wavy water surface, which is the most common scenario. For long distance communication from air to underwater optoacoustic energy conversion is indeed a viable option.

Optoacoustic energy conversion means converting light energy into acoustic energy. Such an energy conversion mechanism was discovered long ago by Alexander Graham Bell in 1881 [5], and could be classified into two categories, linear and nonlinear. In a linear optoacoustic energy transfer, high energy laser pulses only heat that medium. On the other hand, for a nonlinear energy transfer mechanism not only the target medium gets heated but also changes its physical state. In the linear mechanism, the generated acoustic signal is proportional to the input laser power; on the other hand, in the non-linear optoacoustic category, the power of generated acoustic signal varies nonlinearly with the laser power. A nonlinear optoacoustic mechanism requires more laser power than a linear one and yields an acoustic signal that is quite complex to model and characterize. Therefore, this paper focuses only on the linear mechanism. Figure 1 explains the general setup for how we can communicate from air to underwater using optoacoustic energy conversion method. A high energy pulsed laser is required for this kind of setup. Typically, Q-switch Nd:Yag laser is good for this application.

Optoacoustic energy conversion methods are very popular in medical applications, especially in medical imaging [6][7]. Nonetheless, its usage for underwater communication is still in infancy stages. Only few studies have been made on laser generated sound in the water medium by optoacoustic energy conversion methods. In [8], a time and frequency domain analysis have been conducted on the generated acoustic signal in the water medium. Such analysis has also shown the angular dependency of the sound pressure level for the oblique laser

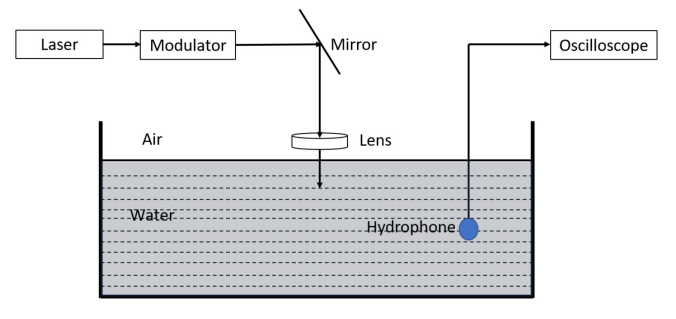


Fig. 1. A block diagram description of establishing optoacoustic communication from air to water.

beam incidence at the air-water interface. Blackmon et al. [9] have investigated the M-ary Frequency Shift Keying (FSK) and Multi-frequency Shift Keying (MFSK) for both linear and nonlinear optoacoustics. To the best of our knowledge, no prior work has focused on how to control the characteristics of the generated acoustic signals, especially for wavy water surfaces.

There is some other notable research on optoacoustic downlink communication from air-to-water. Since the generated acoustic signal is broadband, there is a frequency that carries most of the energy, which is referred to as peak frequency. The relationship between peak frequency and laser power has been discussed in [10]. Such work has pointed out that increasing the laser pulse energy caused a decline in the peak frequency. Generally, low frequency acoustic signals can travel further in an underwater environment. Hence, for long distance underwater communication, we need to provide higher energy laser pulses. Y. H. Berthelot [11] has shown that we can create a narrowband acoustic signal by choosing the laser repetition rate based on the laser parameters. However, the theoretical value of such a repetition rate is several KHz which is normally impossible with available current laser sources in the market [12]. Determining the laser repetition rate to create a narrowband signal also requires knowing the value of incident angle of laser light on the water surface. For a flat-water surface, the value of incident angle is fixed; yet for wavy water surfaces the incident angle continuously changes and makes it impossible to choose a single repetition rate.

In summary, the aforementioned studies have pointed out that the characteristics of the generated acoustic signal, i.e. signal strength and frequency spectrum, would depend on the laser incident angle on the water surface and the observation angle of the underwater node. These angles are continuously changing for a wavy water surface. In this paper, we analyze how to control the acoustic signal characteristics for both flat and wavy water surfaces. We then provide guidelines for the placement of the airborne unit and the underwater node for optimal generated signal quality. Our study shows that the positioning guidelines also hold for rough water conditions with moderate wave amplitude. Our analysis is supported by extensive simulation experiments. Our results are invaluable for establishing robust communication links by enabling effective optoacoustic modulation and controllable bit error rates.

This paper is organized as follows. In section II, we analyze the spectral response of the optoacoustic effect. Section III explains how to optimally position the airborne unit and underwater node for generation of better quality acoustic signal. Section IV discusses the simulation results. The paper is concluded in Section V.

II. THEORETICAL ANALYSIS

We have already mentioned that the generated acoustic signal from an optoacoustic energy transfer mechanism is generally a broadband signal. Therefore, it is important to have the pressure spectral response analysis. In this section, we will discuss the spectral response of the acoustic pressure; based on such analysis, we will determine the best relative position of an airborne unit and underwater node for better quality acoustic

Table 1. A summary of the important notations

Notation	Description
r	Range to the observation point
θ_i	Incident angle
θ_r	Refracted angle
heta	Observation angle from vertical axis
φ	Observation angle from horizontal axis
t_r	Optical transmissivity of the water
β	Thermal expansion coefficient
C_p	Specific heat of the water medium
μ	Optical absorption coefficient
а	Laser beam radius
I_0	Laser intensity amplitude
τ	Laser pulse duration
T	Laser pulse repetition period
I(t)	Temporal laser waveform
$I(\omega)$	Impulse response of laser waveform
k	Acoustic wave number
ω	Angular frequency of acoustic wave
С	Speed of acoustic wave

signal generation. In the next section, we will show how this analysis helps in determining the relative positioning of the airborne unit and underwater node for the wavy water surface using a surface wave modeling function.

A. Acoustic Spectral Response

The pressure spectral response of the generated acoustic signal by optoacoustic energy conversion methods depends on the laser parameters, medium parameters and the range of the underwater node, i.e. position of the hydrophone in the underwater. This pressure spectral response has been calculated by solving Green's function integral for normal [11] and oblique incident [8]. Eq. (1) shows the result for an oblique laser beam incident [8].

$$P(r,\omega) = \frac{-t_r K}{u} \cdot e^{ikr} \cdot I(\omega) \cdot \frac{\Lambda}{u} \cdot \frac{e^{\mathcal{F}}}{\Delta}$$
 (1)

where.

$$K = \frac{i\mu\beta p_0\omega}{4\pi C_0 r},\tag{2}$$

 $K = \frac{i\mu\beta p_0\omega}{4\pi c_p r},$ $\frac{\Delta}{\mu} = 2i\sigma \sin\theta_r \sin\theta \cos\varphi \sinh(\xi) - 2\sinh(\xi) - 2i\sigma \cos\theta \cos\theta_r \cosh(\xi),$

$$2i\sigma\cos\theta\cos\theta\cos\theta_r\cosh(\xi),\tag{3}$$

$$\xi = \frac{k^2a^2\sin2\theta\cos\varphi\sin2\theta_r}{8},\tag{4}$$

$$\Delta = 1 - 2i\sigma \sin\theta_r \sin\theta \cos\varphi + \sigma^2(\cos^2\theta \cos^2\theta_r - \sin^2\theta_r \sin^2\theta \cos^2\varphi), \tag{5}$$

$$\sigma = \frac{k}{n} = \frac{\omega}{n s'} \tag{6}$$

$$\sigma = \frac{k}{\mu} = \frac{\omega}{\mu c'},$$

$$\mathcal{F} = \frac{-k^2 a^2 (\sin^2 \theta \sin^2 \varphi + \cos^2 \theta_r \sin^2 \theta \cos^2 \varphi + \sin^2 \theta_r \cos^2 \theta)}{4}$$
(7)

All the parameters in Eq. (1) to (7) are described in Table 1, and the angles are marked in Figure 2. In Eq. (1), $I(\omega)$ is the

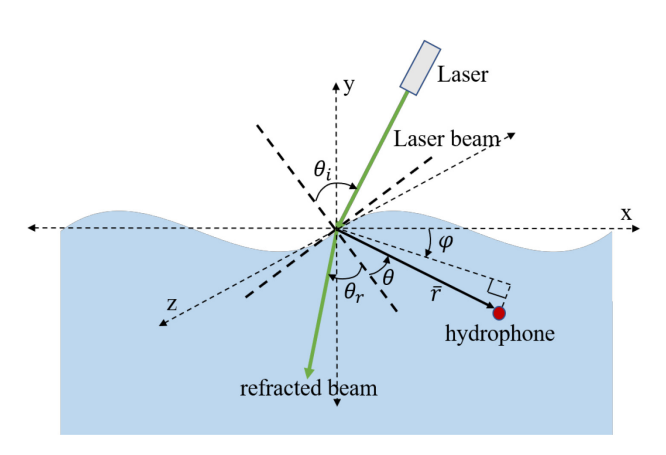


Fig. 2. General geometry for linear optoacoustic communication from air to underwater

spectral response of the laser pulse waveform. Let I(t) be the normalized laser beam profile; it can be represented as follows:

$$I(t) = \sum_{n=0}^{N-1} e^{-(\frac{t-nT}{\tau})^2}$$
 (8)

By applying a Fourier transform on Eq. (8), we get $I(\omega)$, which will be:

$$I(\omega) = \tau \sqrt{\pi} e^{-\frac{\omega^2 \tau^2}{4}} e^{i(N-1)\omega T} \frac{\sin \frac{N\omega T}{2}}{\sin \frac{\omega T}{2}}$$
(9)

where, N is the number of Gaussian laser pulses, T is the laser pulse repetition period and τ is the laser pulse duration. If we know the value of all the parameters listed in Table 1, we can calculate Eq. (2) - (9) and then substitute all values in Eq. (1). Hence, we can calculate the spectral response of the generated acoustic wave.

Through careful consideration of Eq. (1), we can note that there are three types of parameters: laser beam parameters, environmental parameters and some observation angles based on the relative position of laser source, hydrophone and water surface. For a specific laser beam source, the laser beam parameters and environmental parameters are fixed. Therefore, we can divide Eq. (1) into two parts as follows:

$$A_0(\mu, p_0, \omega, r, \tau, T) = \frac{-t_r K}{\mu} \cdot e^{ikr} \cdot I(\omega)$$
 (10)

$$D(\theta_r, \theta, \varphi, \omega, \mu, a) = \frac{\Lambda}{\mu} \cdot \frac{e^{\mathcal{F}}}{\Delta}$$
 (11)

where, A_0 is the amplitude term whose value depends on the optical absorption coefficient, laser beam peak power, communication distance, laser pulse duration and laser pulse repetition rate. Here, D is the directionality factor, which mainly depends on the refracted angle, θ_r , the vertical observation angle, θ , and the angular frequency, ω , of the acoustic wave. The refracted angle, θ_r can be calculated from the laser beam incident angle, θ_i by using Snell's law.

$$\theta_r = \sin^{-1}(\frac{n_a}{n_w}\sin\theta_i) \tag{12}$$

where, n_a and n_w are the refractive index of air and water respectively. Substituting the value of A_0 and D in Eq. (1) we get,

$$P(r,\omega) = A_0 \times D \tag{13}$$

In the next subsection we will briefly describe amplitude, A_0 and directionality factor, D.

B. Parmeter Effect Analysis

Amplitude factor, A_0 : From Eq. (2) and Eq. (10) we can see that the amplitude factor grows with the increase of the power and optical absorption coefficient of the laser beam; yet it decreases with the increase in observation distance. The value of this amplitude factor is plotted in Figure 3(b) with respect to frequency for laser parameters, $p_0 = 2 MW$, $\mu = 13.7 m^{-1}$, $\tau = 10 ns$ and T = 10 ms. From this figure we can conclude that the value of A_0 grows with the increase of frequency.

<u>Directionality</u>, *D*: As we already discussed, the directionality, *D* mainly depends on the relative position of laser light source

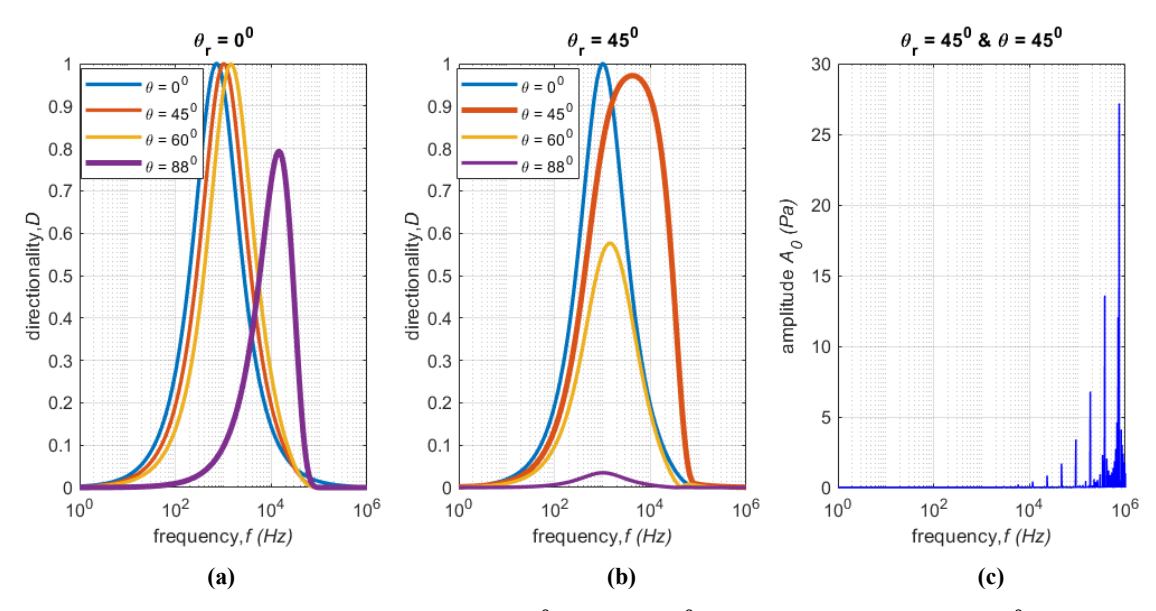


Fig. 3. Determination of directionality factor, D for a) $\theta_r = 0^0$, b) $\theta_r = 45^0$ and amplitude, A_0 c) $\theta_r = 45^0$ and $\theta = 45^0$ for various frequency component of pressure wave

and underwater observation point, i.e. refracted angle, θ_r , and vertical observation angle, θ . Eq. (13) shows that the acoustic pressure value is the multiplication of D and A_0 . Hence, in order to maximize the pressure value, we need to maximize both D and A_0 . Figure 3 shows the simulation results of D for various frequency components of the pressure wave using the same laser parameters that are used to calculate A_0 . This simulation is generated using Eq. (3) - (7) and Eq. (11). Figure 3(a) plots D with respect to f for various settings of θ while $\theta_r = 0^0$. The figure indicates that increasing f boosts the value of D until a certain level after which D starts to decline. Basically, the directionality factor, D acts like a band pass filter, whose lower and upper cut-off frequencies depend on θ . In addition, Figure 3(a) shows that the gap between the lower and upper cut-off frequency widens with the increase of θ . For example, when $\theta = 0^{0}$, the frequency response spans from few Hz to approximately 10 kHz. On the other hand, when $\theta = 88^{\circ}$, the frequency response covers from few Hz to approximately 100 kHz. From Figure 3(c), we observe that the value of A_0 is almost zero up to 10 kHz. So, in this setup if we choose $\theta =$ 88^{0} , we can maximize the product of D and A_{0} , and hence we can maximize the value of p. Keep in mind that Figure 3(a) has been drawn for $\theta_r = 0^0$. We have increased θ_r , specifically, $\theta_r = 45^{\circ}$, and recalculated D; the results are plotted in Figure 3(b). The figure shows the maximum frequency span when $\theta =$ 45°. Based on Figures 3(a) and 3(b), we realize that, in order to maximize the value of p, we need to choose θ and θ_r in such a way that the sum of these two angles is close to 90° . If γ is the sum of these two angles then,

$$\gamma_{D_{max}} \approx \theta + \theta_r$$
 (14)

We can further validate Eq. (14) from Figure 4, which shows the value of D for various θ while keeping θ_r fixed. In Figure 4(a), $\theta_r = 0^0$, and hence we get maximum D when θ is close to 90^0 . On the other hand, in Figure 4(b), D is maximum when $\theta = 30^0$ and $\theta_r = 60^0$. Based on this finding, in the next

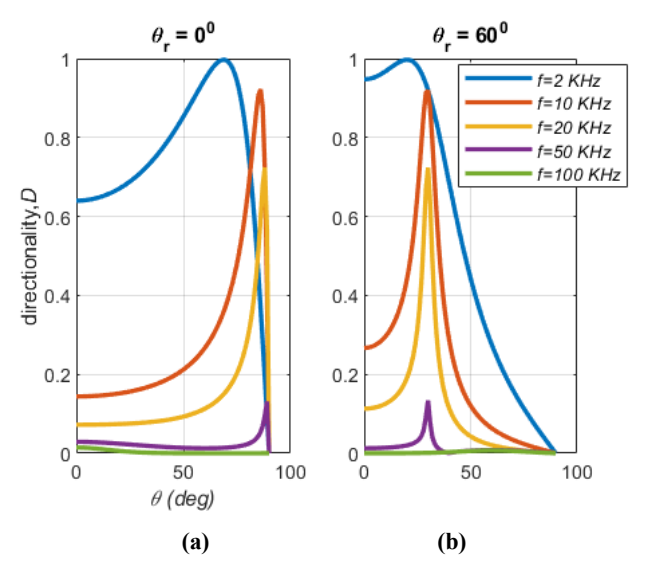


Fig. 4. Directionality, D vs vertical observation angle, θ for (a) $\theta_r = 0^0$ and (b) $\theta_r = 60^0$

section we will discuss how to exploit the relationship between the position of laser source and the underwater observation point for improving the quality of acoustic signal for both flat and wavy water surfaces.

III. POSITIONING OF AIRBORNE AND UNDERWATER NODES

The theoretical analysis in the previous section has highlighted the importance of selecting θ and θ_r and how keeping the sum of their values around 90^0 improves the quality of the generated acoustic signal. Based on such analysis, if we know the underwater node position, i.e., hydrophone position, we can shoot the laser beam in such a way that it creates the desired value of θ_r . Now based on the value of such θ_r , we can calculate the incident angle, θ_i using Eq. (12). In this section, we discuss optimum positioning of the laser source and underwater node for both flat and wavy water surfaces.

A. Flat water surface

For a flat water surface, it is easy to calculate all the angle values; these angles do not change over time since the water surface is flat. Figure 5 shows some good relative positions of the laser source and the underwater node. For example, if the underwater node position is such that it creates 45° angle with the laser beam incident point at the water surface, we need to shoot the laser beam at such an incident angle so that the refracted angle becomes close to 45° as well. This scenario is explained in Figure 5(a). Figure 5(b) shows the best shooting angle of the laser beam for an underwater node close to the water surface. Similarly Figure 5(c) shows the best angle values for underwater nodes, which is vertically below the laser beam incident point at the water surface.

B. Wavy water surface

For a wavy water surface all angles continuously change over time due to waves on the water surface. In order to calculate these angles, we need to know the water surface function. It is very difficult to accurately model the water surface function. The simplest way to model the water surface is to assume that it is trigonometric function, e.g., sin or cosine, with variable amplitude and frequencies. However, more complex and accurate surface models exist in the literature. Typically, a surface of open water resembles a conoidal function. A conoidal function has relatively higher crest and flatter trough than sine function. Modeling of water surface also depends on the water depth. Boussinesq equations and Korteweg—de Vries equation (KdV) are the popular mathematical models for the water surface when the water depth is shallow [13]. On the

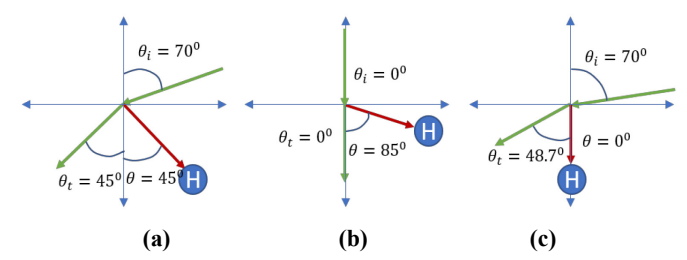


Fig. 5. Relative position of laser beam incident point and hydrophone position for better quality pressure wave

other hand, Stroke's wave theory is used to determine the water surface function for deep water [14]. In [15] and [16] these models are explained mathematically with detailed analysis. We utilize those calculations to simulate the water surface model in the simulation section.

Now, using any of the water surface models described above, we can calculate the value of θ , θ_i , and θ_r at a particular phase or time of the water surface function. Again, we want to shoot the laser beam at such an angle so that the generated acoustic signal's strength is maximal for a known position of an underwater node. To find such an angle, we will start with an optimal position of the laser source and underwater node for a flat water surface and will observe the effect of water waves on the relative positions of the communicating pair. Figure 6(a) shows the optimal value of these angles for the particular hydrophone positions. If the water surface is wavy, these angles will be changing continuously over time. Figure 6(b) shows the angle values at a particular phase (moment of time) of the water surface. At this particular moment, we can observe that the value of θ_i , and θ_r becomes larger in comparison to the flat surface scenario. However, the value of θ becomes smaller than the flat surface. In essence, the sum of θ and θ_r remains almost the same, which is close to around 90°. This is a very important finding and is consistent with Eq. (14). interesting question is whether this holds for a full wave period, i.e., at any particular moment of the water surface. In order to answer such a question, we need to calculate the values of θ and θ_r for all phases of a water surface period. The results are shown in Figure 7. This figure plots the sum of θ and θ_r for all phases of a water surface for different wave amplitudes. Based on these results, we can note that when the wave amplitude is zero, i.e., the water surface is flat, the sum of these angles is 90° which is as expected from the above analysis. With the variation of water surface amplitude, the fluctuation of $\theta + \theta_r$ stays around 90°. If the water wave amplitude increases the deviation from 90° also grows, which has been shown in Figure 7 for four different wave amplitudes. Typically, water waves are not high in most setups under normal environmental conditions. Some rough wave crests could exist at shores and during environmental hazards like Tsunami, cyclone, etc. Therefore, we can conclude that the optimum relative positions of the laser source and underwater node for flat surface are still applicable for a wavy water surface in most practical scenarios. We confirm such a conclusion in the next section.

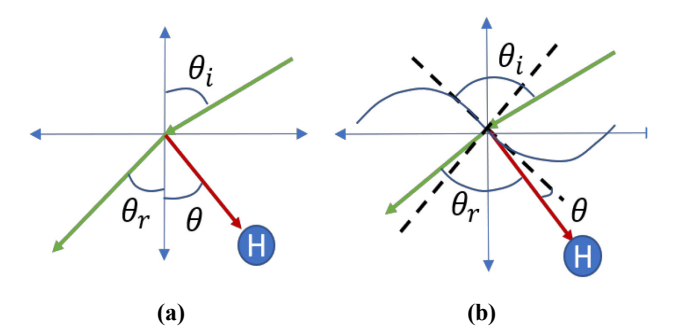


Fig. 6. Relative position of laser beam incident point and hydrophone for (a) flat and (b) wavy water surface

IV. VALIDATION RESULTS

From the previous section, we know that in order to create a relatively strong narrowband signal, we need to choose θ and θ_r such that their sum remains close to 90°. In this section, we simulate the spectral response of the generated acoustic signal using Eq. (1) - (9) for both flat and wavy water surfaces. The simulation results for flat water surface are shown in Figure 8 for various values of θ and θ_r while keeping other laser and environmental parameters fixed. The laser parameters have been chosen based on a currently available laser source [12]. Basically, we have set, $\mu = 13.7 \, m^{-1}$, $\beta = 210 \times 10^{-6}$ $(1/{}^{0}C)$, $p_0 = 2 \times 10^{6} \text{ MW/m}^2$, a = 3 mm, $C_p = 4200 \text{ J/Kg.k}$, r = 1 m, $\tau = 10 ns$, T = 10 ms and c = 332 m/s. Figures 8(a) and 8(b) show that when the sum of θ and θ_r is not 90°, the spectral response is very broadband, spanning from few Hz to 1 MHz, and the pressure spectral amplitude is very low with a maximum around 50 mPa. On the other hand, Figures 8(c) and 8(d) indicate that the pressure spectrum spans from few Hz to approximately 100 KHz and the maximum spectral amplitude is around 350 mPa. Hence, in these cases, the frequency spectrum is almost 10 times lower than the Figures 8(a) and 8(b). Moreover, the maximum spectral amplitude is also higher than that in Figure 8(a) and 8(b). In essence, we are getting a relatively narrowband signal with high spectral amplitude response when θ and θ_r are chosen such that their sum is 90°.

In the previous section, we have concluded that the criterion of choosing θ and θ_r for a wavy water surface is similar to that of the flat-water surface for typical water wave fluctuations. To confirm such a conclusion, we show in Figure 9 the simulation results for the spectral response of the generated acoustic signal corresponding to a wavy water surface. This simulation has been conducted for various phases of the wavy water surface function while fixing the amplitude of the water wave at 30 cm. The results in this figure are almost similar to those in Figures 8(c) and 8(d) for various phases of the wavy water surface. Yet, the amplitude of spectral response becomes a bit weaker than the flat water surface which is expected because the sum of θ and θ_r is not anymore 90° due to the fluctuation of wavy water surface, as shown in Figure 7. If the water surface amplitude increases, the deviation of the sum of θ and θ_r from 90° will

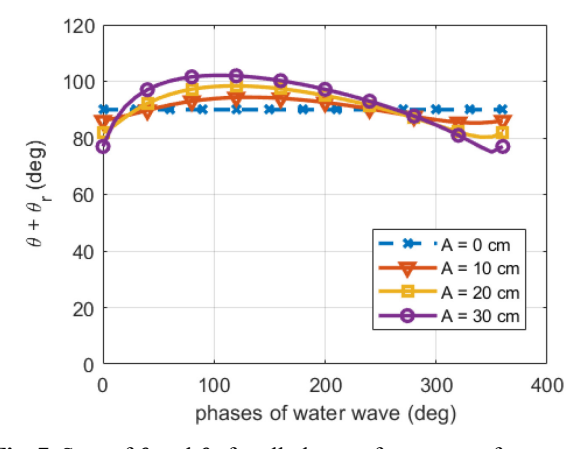


Fig. 7. Sum of θ and θ_r for all phases of a water surface wave. Here water surface is assumed to be a sine wave

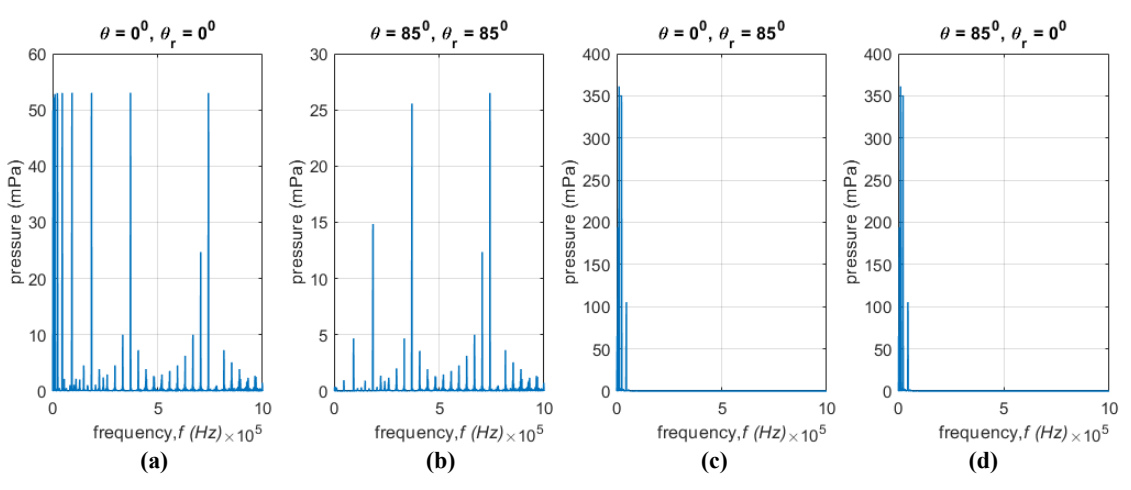


Fig. 8. Spectral response of acoustic wave, for (a) $\theta_r = 0^0$, $\theta = 0^0$, (b) $\theta_r = 85^0$, $\theta = 85^0$, (c) $\theta_r = 85^0$, $\theta = 0^0$, and (d) $\theta_r = 0^0$, $\theta = 85^0$

also increase; hence the amplitude of spectral response will decrease where Figure 8 shows that if the sum of θ and θ_r is not 90°, the spectral amplitude decreases.

V. CONCLUSION

This paper reports a study of the effect of the laser beam incident angle and observation angle on the spectral response of the generated acoustic signal using linear optoacoustic methods. The study has provided guidelines on optimum positioning of airborne and underwater nodes for which we can generate the best quality acoustic signal. The best quality implies an acoustic signal that has the highest spectral response at the lower frequency components. Low frequency acoustic signals are preferred since they can travel long distances in the water medium. Through theoretical analysis and simulation, we have shown that if the sum of the refracted angle of the laser beam in the water medium and the observation angle of the underwater node from vertical axis is around 90°, we can create a relatively narrowband signal with high signal strength. The results of our study are paramount for establishing robust

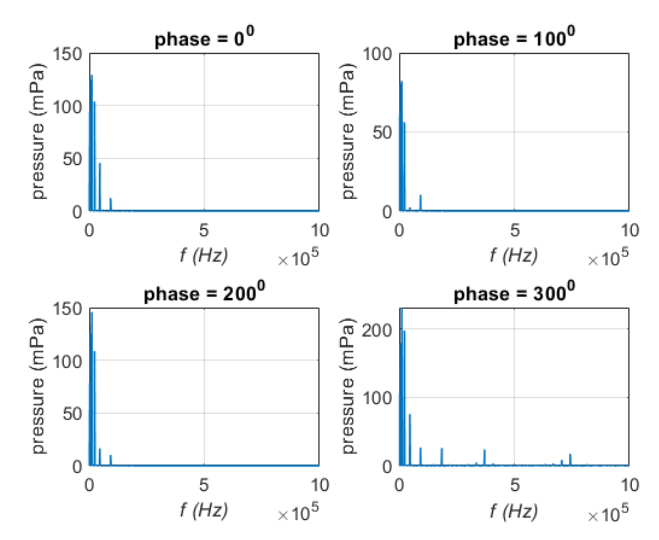


Fig. 9. Spectral response of acoustic signal for various phase of the wavy water surface while wave amplitude = 30 cm

communication links that leverage the optoacoustic effect and serve applications where underwater nodes need to be reached without employing gateway nodes on the water surface.

<u>Acknowledgment:</u> This work is supported by the National Science Foundation, USA, Contract #0000010465.

REFERENCES

- [1] G. F. Edelmann, T. Akal, W. S. Hodgkiss, Seongil Kim, W. A. Kuperman and Hee Chun Song, "An initial demonstration of underwater acoustic communication using time reversal," *IEEE Journal of Oceanic Engineering*, 27(3), pp. 602-609, July 2002.
- [2] S. Sendra, J. Lloret, J. M. Jimenez and L. Parra, "Underwater Acoustic Modems," *IEEE Sensors Journal*, 16(11), pp. 4063-4071, June 2016.
- [3] M. S. Islam and M. F. Younis, "Analyzing visible light communication through air–water interface," *IEEE Access*, 7, pp. 123830-123845, 2019.
- [4] C. J. Carver, et al., "AmphiLight: Direct Air-Water Communication with Laser Light," Proc. USENIX Symposium on Networked Systems Design and Implementation (NSDI), 2020.
- [5] A. G. Bell, "Upon the production of sound by radiant energy," Philos. Mag. Ser. 5 11, 510, 1881.
- [6] A. Vogel, J. Noack, G. Hüttman, et al. Mechanisms of femtosecond laser nanosurgery of cells and tissues. *Appl. Phys. B* 81, 1015–1047, 2005.
- [7] A. Vogel, S. Busch, and U. Parlitz, "Shock wave emission and cavitation bubble generation by picosecond and nanosecond optical breakdown in water," J. Acoust. Soc. Am., 100, pp. 148-165, 1996.
- [8] F. Blackmon, L. Estes, and G. Fain, "Linear optoacoustic underwater communication," Appl. Opt., 44, pp. 3833-3845, 2005.
- [9] F. Blackmon, L. Antonelli, "Remote, aerial, opto-acoustic communications and sonar," Proc. SPIE 5778, Sensors, and Command, Control, Communications, and Intelligence (C3I) Technologies for Homeland Security and Homeland Defense IV, (20 May 2005).
- [10] T.G. Jones, M. Helle, A. Ting, and M. Nicholas, "Tailoring Underwater Laser Acoustic Pulses", 2012.
- [11] Y. H. Berthelot, "Thermoacoustic generation of narrow-band signals with high repetition rate pulsed lasers," J. Acoust. Soc. Am., 85, pp. 1173–1181, 1980
- $[12]\ www.quantel-laser.com/en/products/item/ultra-50-100-mj--134.html$
- [13] E. Infeld, A. Karczewska, P. Rozmej, "Solutions to the extended KdV equation for water surface waves," *Nonlinear Dynamics*, 91(2), pp 1085–1093, January 2018.
- [14] R. Wiegel, "A presentation of cnoidal wave theory for practical application," J. of Fluid Mechanics, 7(2), pp. 273-286, 1960.
- [15] M. W. Dingemans, "Water wave propagation over uneven bottoms," World Scientific, pp. 708-715, 1997.
- [16] M. Davies, and A. Chattopadhyay, "Stokes Waves Revisited: Exact Solutions in the Asymptotic Limit," *The European Physical Journal Plus*. 131. 10.1140/epjp/i2016-16069-7, 2016.